Inertial and Digital Stabilization for LEO and GEO Missions

N. Guercio[(1)], S.Henrot[(1)], T.Chambon[(1)], F.Boquet[(2)], N.Deslaef[(2)], D.Alazard[(4)], F. Sanfedino[(4)], L.Berrojo [(3)], E. Muñoz De La Torre[(3)], P. Spanoudakis[(5)], J. Rouvinet[(5)] A. Torasso[(6)]

(1) Thales Alenia Space – 5 Allée des Gabians, 06150, Cannes (France); (2) ESA/ESTEC – Keplerlaan 1, 2201AZ, Noordwijk, ZH (Netherlands); (3) Thales Alenia Space - C. de Einstein, 7, 28760 Tres Cantos, Madrid, (Spain);
(4) ISAE Supaero - 10 avenue Edouard Belin, Toulouse (France); (5) CSEM, Rue Jaquet-Droz 1, 2002 Neuchâtel, (Switzerland); (6) Innalabs, Snugborough, Dublin, (Ireland);

ABSTRACT

Line Of Sight (LOS) Stabilization techniques are a strategic topic, as they enable high pointing performance missions and can provide relaxation to platform stability requirements that can lead to major cost reductions. The maturity of space industry allows the development of standard platforms that are now more and more often considered as commodities. In such a context, the concept of hosted payload is becoming a standardized approach and the development of active line of sight concepts part of the payload becomes central. The first part of the paper presents a LEO push-broom interferometer agile mission implementing inertial based opto-mechanical stabilization. A dedicated breadboard allowed validating the approach and increasing the maturity of the stabilization system, confirming expected performances. The second part of the work presents the design and performance assessment of a digital stabilization system for a multispectral imaging mission from GEO orbit, using a process called multi-frame super-resolution. The method performance is assessed, and its sensitivity to the main design drivers is derived showing that it is compliant to the requirements over a variety of conditions.

1 INTRODUCTION

Earth Observation and Science High Accuracy pointing missions involve platforms with highly stable structural, thermal, and dynamic environment in order to meet image stability requirements. This is accomplished by utilizing solutions that range from sensing level to actuation level, including high-performance Star Trackers and gyros, Fine Guidance Sensor embedded in the Payload, and low noise actuators, like isolated Reaction Wheels and cold gas propulsion[11][12]. Active or passive isolation of instruments is also possible to reduce vibrations [13].
A different approach consists in stabilizing the line-of-sight stabilization system by using fast steering mirrors inside the instrument to supplement the platform AOCS pointing. This has been successfully implemented in Laser Communication Terminals, Solar Dynamics Observatory, the James Webb Space Telescope [8], GOES-R[14], as well as in Europe for the European Polarimetric and Helioseismic Imager for Solar Orbiter [15]. Several ESA –Thales Alenia Space studies focused on image based line of sight stabilization for GEO high resolution missions [3][4] to reach unpaired performances even with highly stable platforms. The first application of the paper uses these techniques but with inertial sensor measurements. An alternative approach is digital stabilization, which utilizes digital concepts to stabilize images without requiring additional actuators. The

concepts can be broken down in two categories: digital displacement correction, using exposures shorter than the integration time [22][23], or methods tackling frequencies higher than the integration time, such as lucky imaging [16] or deconvolution based approaches. This paper focuses on the former category and presents a shift-and-add super-resolution technique [24][25].

2 INERTIAL LINE OF SIGHT STABILIZATION SYSTEM

2.1 The Mission

The application case studied is a static interferometer mission designed for the analysis of the atmosphere that realizes interferometric acquisitions in both multiple spectral channels. The acquisition procedure is shown in Figure 1, with or without guidance for the slowdown.

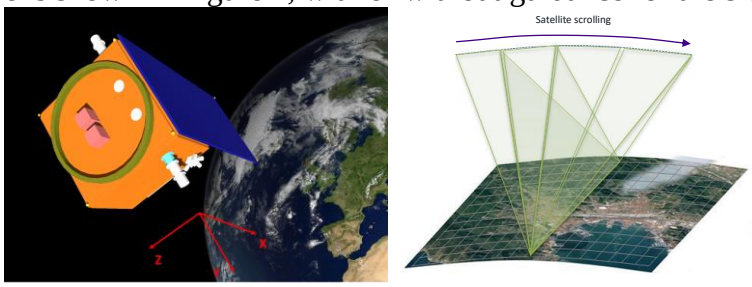

Figure 1 : Overview of the push-broom interferometer mission platform and acquisition principle

The mission should therefore provide the appropriate level of agility to perform measurements at specific locations (+/-100km on ground). Then, the instrument acquires data in push-frame way, thus using high frequency matrix sensors. The scrolling direction corresponds to the optical path differences direction of the interferometers. The goal stabilization requirement are the relative performance error (RPE) over 8.4s, below 2.1µrad and an agility of 20° over 0.7s.

2.2 Stabilization System design

This section presents the stabilization system design for the static interferometer mission.

2.2.1 Architecture

The stabilization system combines both the attitude control system and the line-of-sight stabilization. The platform considered is a low-cost standard platform without high accuracy pointing.

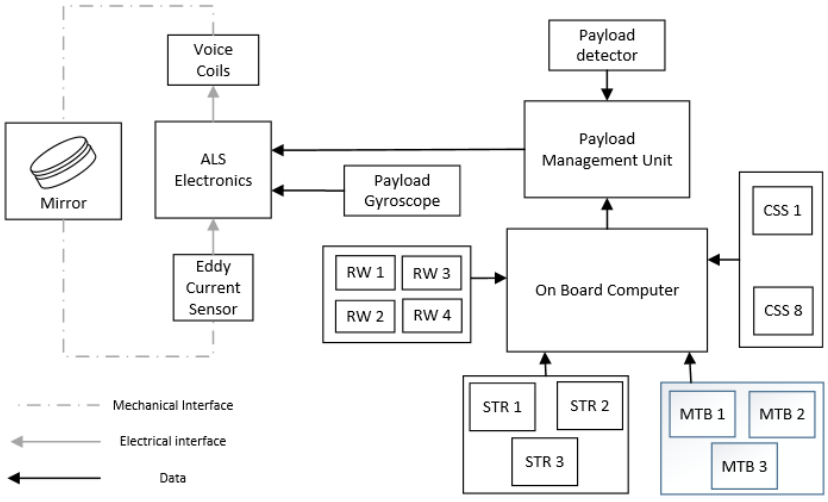

Figure 2: Overview of the AOCS and active LOS (ALS) architecture

The AOCS uses classical equipment such as a 3 optical head star tracker and 4 reaction wheels in a pyramid configuration for the attitude control actuation, offloaded by magneto torquer bars. The stabilization system consists of a second stage based on inertial measurement performed by a gyroscope and an actuator consisting of a SCAN mirror. The AOCS is managed by the on-board computer, while the payload management unit performs the acquisition of the Payload images and the management of the Active LOS (ALS) electronics. The ALS electronics performs the gyroscope and the Eddy Current sensors acquisition, and the command of the voice coil actuators of the scan mirror.

2.2.2 Gyroscope

The gyroscope considered for the Line-of-Sight stabilization system is a Coriolis Vibratory Gyroscope developed by Innalabs modified in the frame of the High Accuracy Image Stabilization Breadboarding Study [2]. The following figure shows an overview of the gyroscope with its performance.

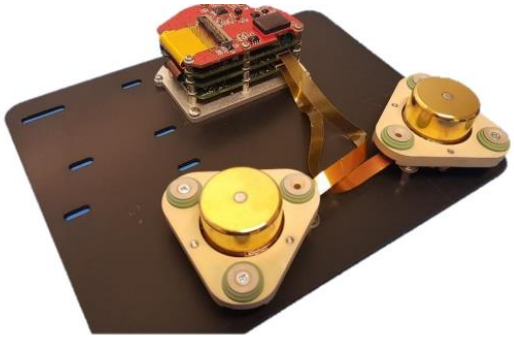

Parameter	Unit	Value
Output signal rate	Hz	8000
Measurement range	deg/s	+/-1
Bandwidth	Hz	150
Angle Random Walk	deg/sqrt(hr)	0,002
Bias stability	deg/hr	0,02
Quiescent Noise 1-100Hz	deg/s	0,01

Figure 3: Overview of the gyroscope sensitive elements and electronics

For the Line-of-sight stabilization system, the low frequency measurement of the gyroscope due to the angle random walk and the Bias Stability should be filtered to avoid the drifting of the SCAN mirror.

2.2.3 Scan mirror

The following figure shows an overview of the mirror designed for the system. The mirror performs the line-of-sight stabilization, the spacecraft instrument pointing in the across-track direction and the instrument slowdown in the along-track direction.

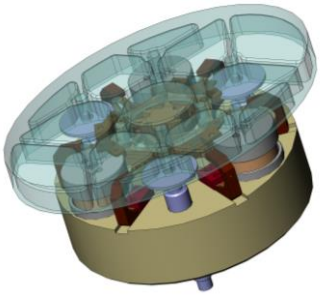

Figure 4 : Scan mirror used for the interferometer application

The SCAN has an elliptical SiC mirror, mounted on a flexible membrane and it is controlled by 3 voice coil actuators spaced 120° of each other. The position is controlled in closed loop using 3 Eddy current sensors in the same configuration. The scan provides +/-10° of range and a very high resolution to ensure a good line of sight stabilization.

2.3 Dynamics modelling

The system dynamics has been developed using the Satellite Dynamics Toolbox [26][27] and takes into account the spacecraft rigid dynamics, the solar array flexible appendage, the reaction wheel rotation dynamics and the flexible scan mirror. Hereafter the figures present the transfer function from spacecraft and scan mirror torques to spacecraft attitude and line of sight. The mirror dynamics uncertainties on the mirror inertia and on the first resonances are included in the control synthesis.

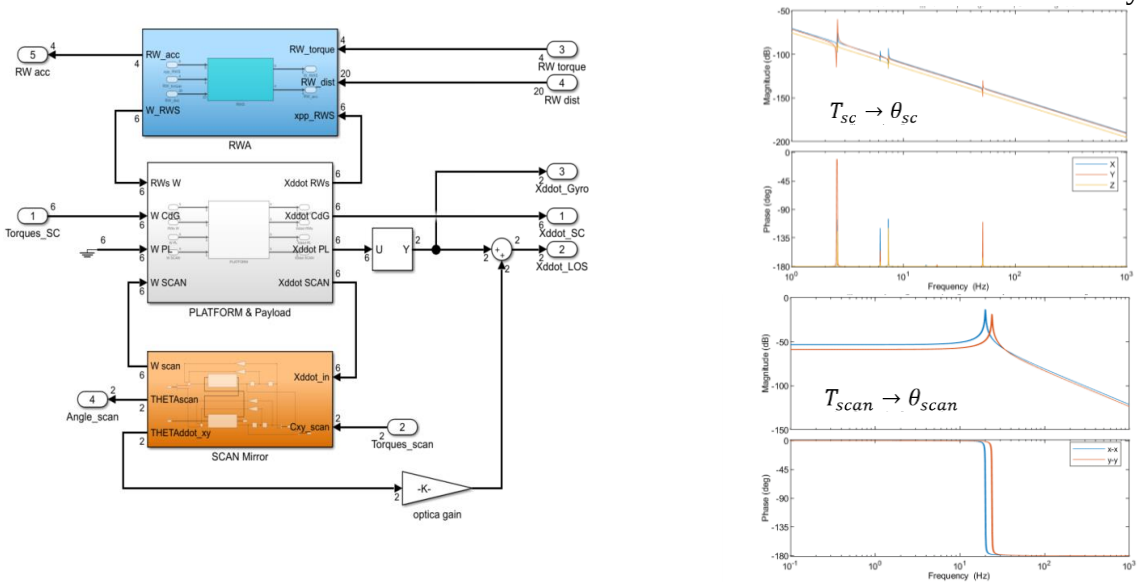

Figure 5: Attitude and line of sight dynamics overview

2.4 Controller design

The control system synthesis model is presented in Figure 6: Overview of the controller architectureFigure 6.

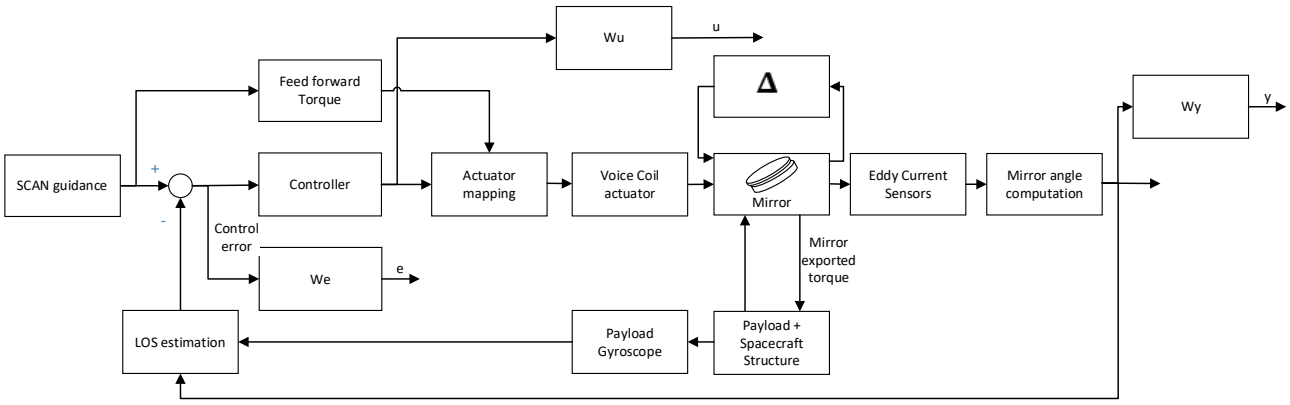

Figure 6: Overview of the controller architecture

The Robust Control Toolbox has been used for the controller design to provide a disturbance rejection bandwidth at -3dB of 10Hz, for agility performance, to be robust to model uncertainties, and to minimize the reinjected sensor noise. Figure 7 shows the control tuning synthesis results, with the requirements, for the sensitivity, complementary sensitivity, and command functions on the left, and the scan agility results on the right.

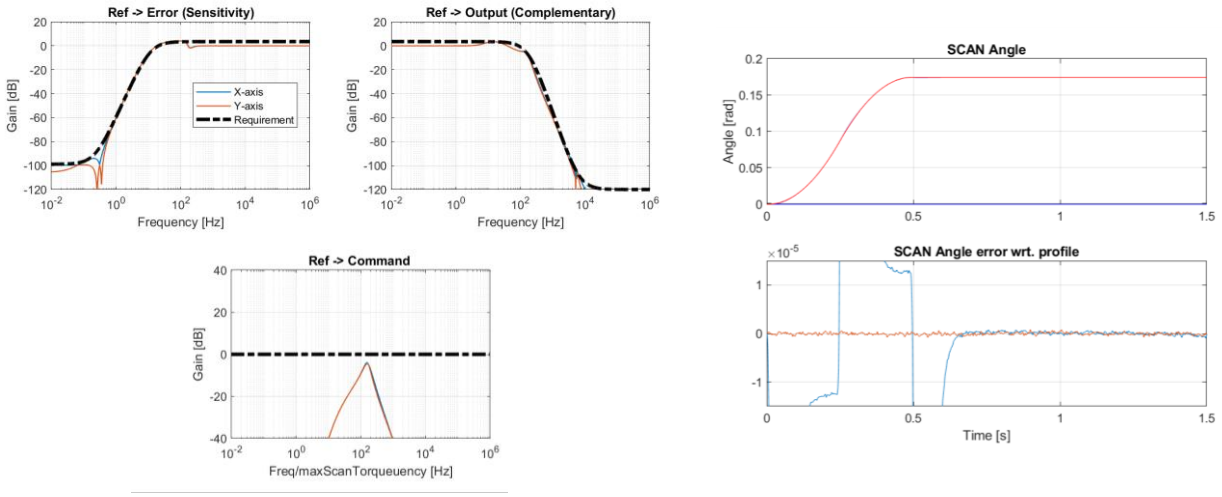

Figure 7: Control tuning results and agility performance

2.5 Simulation and performance assessment

This section gives an overview of the simulator development and the main performance results.

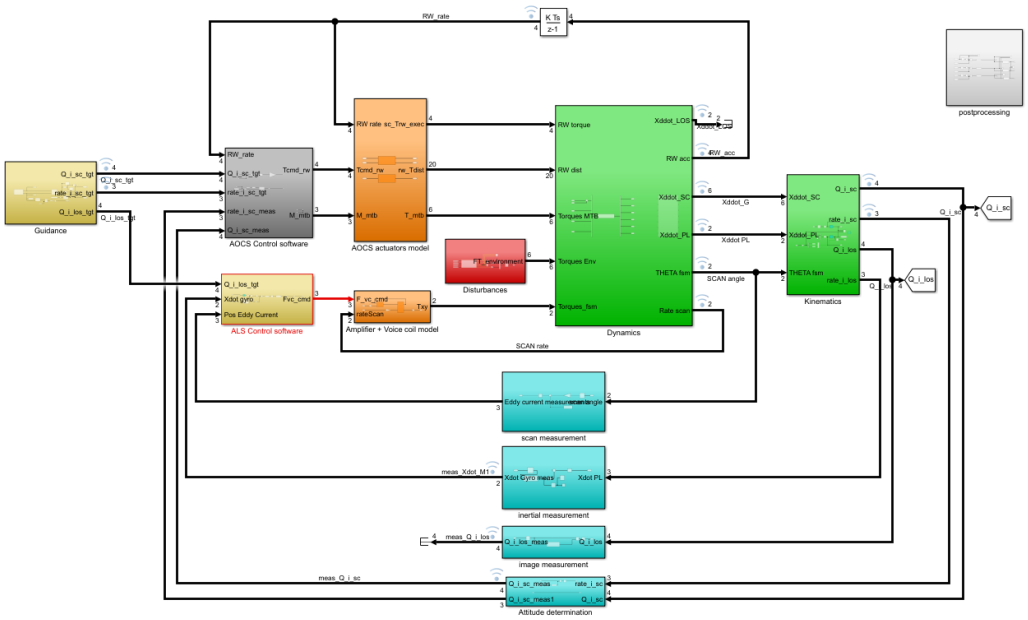

Figure 8: Overview of the platform AOCS and ALS simulator

The simulators implements the Dynamics and Kinematics, the sensors and actuators for the AOCS and the Scan mirror, as well as estimation and control algorithms. The opto-mechanical stabilization system for the push-broom application provided good results with respect to the platform stability concerning the stability performance over 8.4-16.8s, especially with an important fast scan agility. The designed solution is particularly interesting since it provides a good stability (<3 µrad) with a medium performance platform, using a relatively low-cost gyroscope and an accurate scan mirror. It is interesting to note that the main driver is the AOCS residual for the stability over 8.4s and that the system provides good stability in the 10mHz-3Hz bandwidth with a nominal nadir pointing without agility.

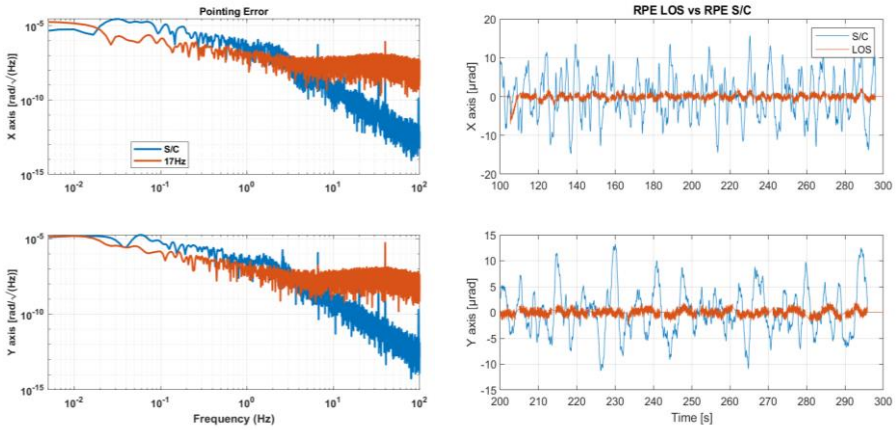

Figure 9: Opto-mechanical stabilization simulation results

2.6 The ISABELA breadboard

The dedicated inertial stabilization breadboard has been developed in the frame of the study [2] for the static interferometer application. The breadboard elements are depicted hereafter.

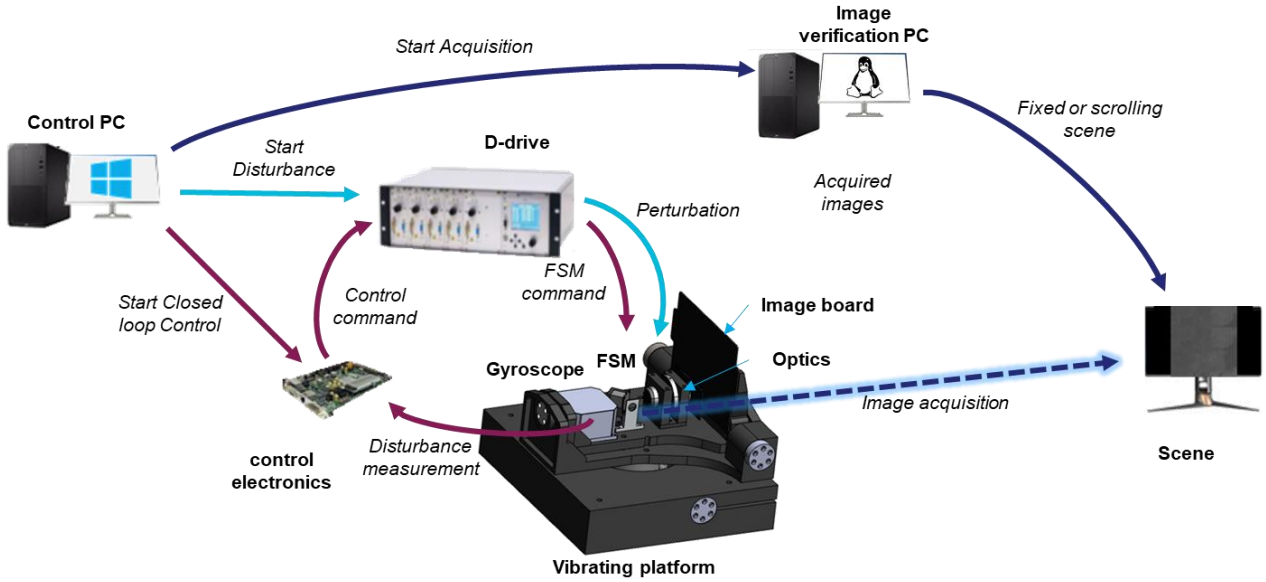

Figure 10 : Breadboard architecture

One can find the different components:

- Vibrating platform: it generates disturbances for the gyroscope and the camera in order to reproduce the Line of Sight residual error of a typical AOCS.
- The Active LOS system consisting in the gyroscope mounted on the platform, a piezoelectric fast steering mirror and the control electronics based on FPGA.
  The verification system consisting in: a high frequency camera with its optics representative of the mission, a screen projecting the observed Earth scene, and the image processing algorithm implemented on the control computer.

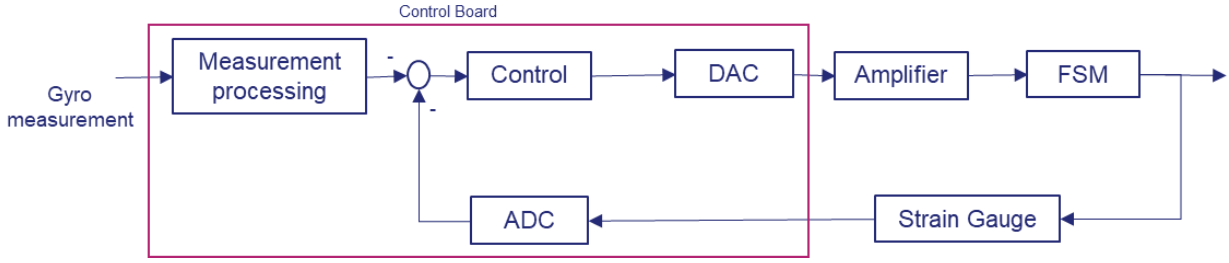

Figure 11 : Breadboard controller architecture

The following figures present the results in open loop and in closed loop in terms of APE and RPE8.4s with a disturbance profile generated with the mission simulator.

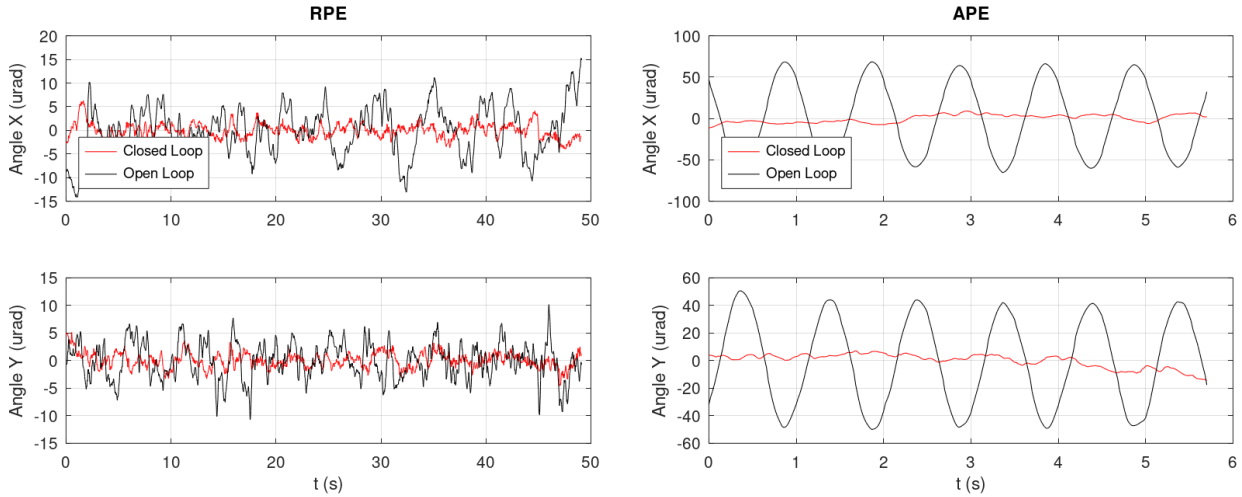

Figure 12: RPE 8.4s (left) and SADM disturbance (right) test with and without ALS

3 DIGITAL STABILIZATION SYSTEM

3.1 The mission

The mission targets the launch of a recurring instrument embedded on a geo-stationary platform providing agility to cover the areas of interest, based on the use of a pointing mechanism at the interface between satellite bus and instrument. The imaging instrument uses off-the-shelf sensors with limited full well capacity. The acquisition phases are separated by slews for instrument pointing, typically up to 10 to 30secs. Therefore, time slots are available for image post-processing. Typical stability requirements are 0.2µrad over up 10 to 100msec depending on the enlightenment of the scene. Platform perturbations affecting the line-of-sight stability are the reaction wheels, Solar Array Drive Mechanism (perturbations up to a few Hz), and the pointing mechanism tranquilization duration: in particular when the instrument pointing is not negligible with respect to platform inertia. Digital stabilization is well adapted to this context with its low recurring cost, reduced data rate and low impact on the existing platform. The mission will benefit from multi-frame super-resolution to increase the final resolution of delivered images.

3.2 Super resolution principle

Digital stabilization relies on multiple acquisitions of the same scene: the high-resolution (HR) image. It is captured on a sensor matrix which is under-sampled with respect to the Shannon-Nyquist sampling theorem: the sensor pixels are too large to capture the highest spatial frequency details. In the Fourier domain, the image contains frequencies beyond the sensor bandwidth: each frame is aliased, i.e. high-frequency details appear as low-frequency patterns. These patterns are different for

each frame, as their sampling grids differ by sub-pixel shifts. This allows to recover high-frequency content from the stack of frames to some extent: this is the multi-frame super-resolution (SR) problem, illustrated in Figure 13.

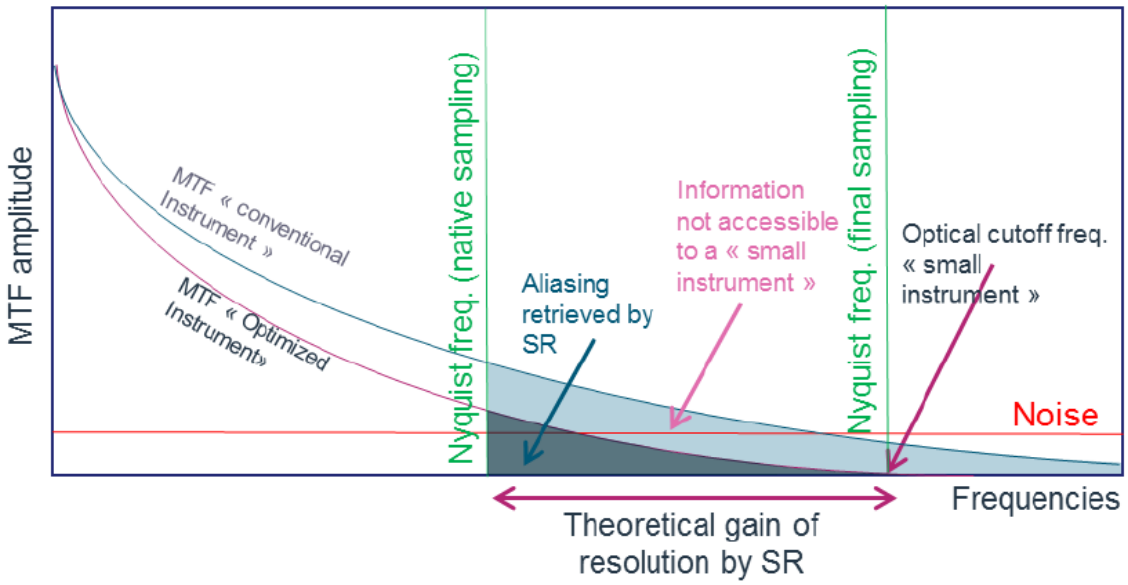

Figure 13 : Illustration of Super-resolution information gain and limitation. SR can theoretically allow to retrieve the complete information acquired by the instrument before sampling. But the results are limited by the noise level. SR cannot go beyond the physical limits of instrument MTF content.

The actual native GSD at instrument level (corresponding to the instrument focal length) will be optimized depending on the performances of the super-resolution algorithm. The greater this GSD is, the bigger will be the instrument field of view. Figure 14 illustrates how this compromise affects system performances and sub-system behavior.

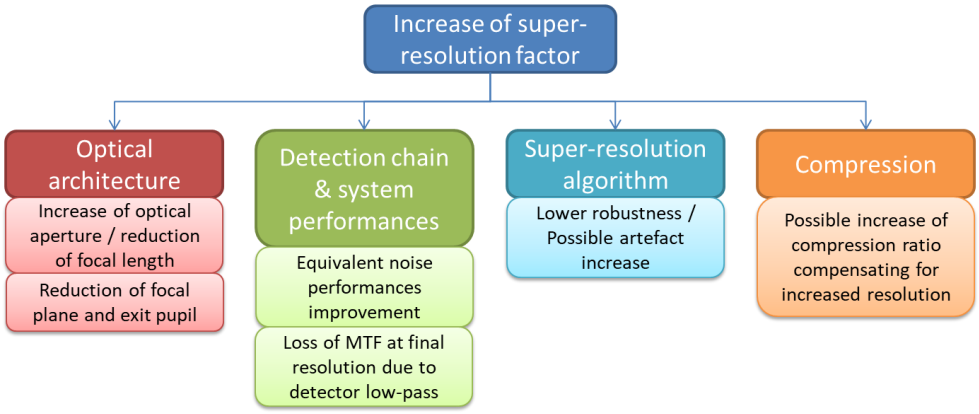

Figure 14 : Impact of focal length (equivalently, super-resolution factor) on system performance

The mission sensor uses a color-filtered arrays (CFAs) following the Bayer pattern to capture several colors on the same matrix, as illustrated in the left part of Figure 15. In this case, SR is coupled with the demosaicing problem, which consists in reconstructing a full color image (right part of Figure 15).

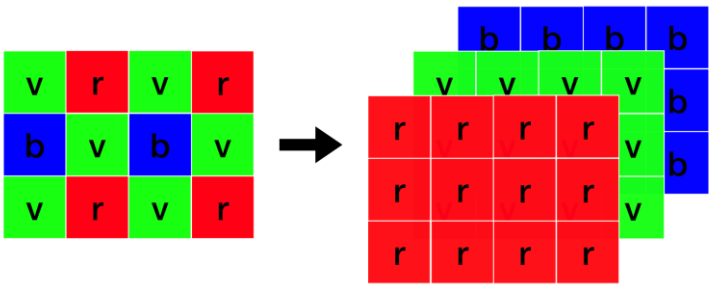

Figure 15 : Demosaicing problem: a RGB image is computed from a Bayer acquisition.

3.3 Digital Stabilization System design

3.3.1 Multi-frame super-resolution algorithm

The Bayer multi-frame super-resolution problem has been tackled by smartphone manufacturers. A state-of-the-art approach was developed by Google as the basis of the digital zoom feature, as well as the default merge method in Night Sight mode (whether zooming or not) on their flagship phone [18]. First, each frame is registered at a pixel level by seeking similar image patches in a pyramidal decomposition; three iterations of Lucas-Kanade optical flow are then performed to achieve sub-pixel precision (see [7]).

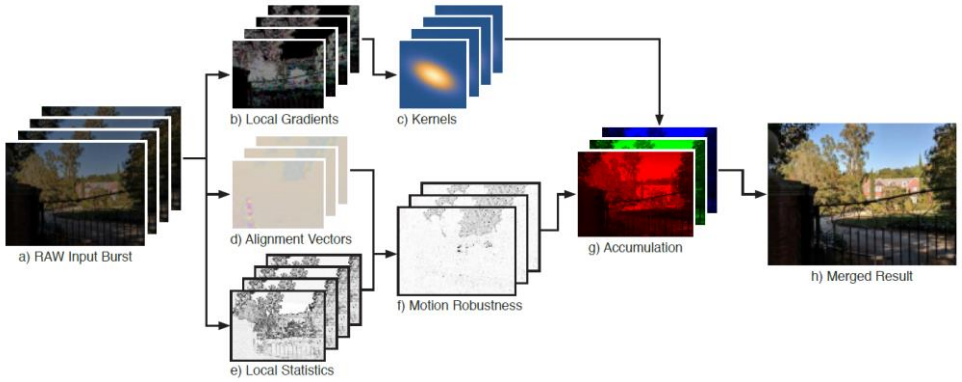

Figure 16: General architecture of the retained multi-frame super-resolution method; from [18]

The fusion of registered frames is accomplished independently for each color component by a weighted 3x3 patch sum. The weights are computed using a Gaussian kernel whose covariance matrix is derived from the local gradient, and a local robustness factor is accounted for e.g. to prevent merging moving objects and alignment failures.

3.3.2 Algorithm robustness

In the Google approach, robustness is achieved by computing a factor weighting the contribution of local pixel contributions for all frames during the fusion process. This robustness factor accounts for local statistics and color differences. According to this factor value, the likelihood of a frame being either misaligned or too noisy can be evaluated, and a fusion decision can be made, as illustrated in Figure 17.

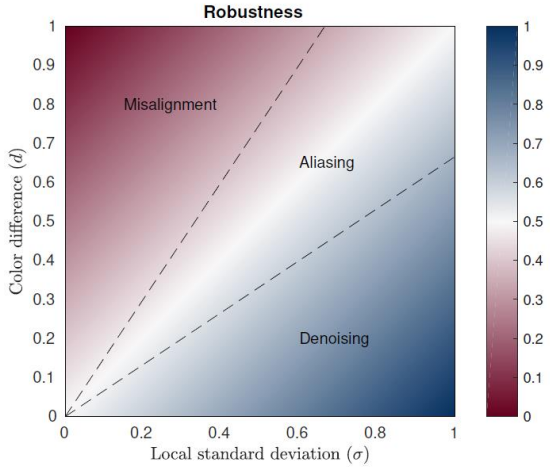

Figure 17 : Google statistical robustness model: the relationship between color difference d and local standard deviation σ dictates the merging of a given frame with respect to the base frame; from [18].

3.4 Experimental results

A specific simulation tool has been developed in the frame of the study to assess the performance over representative images, with the sensitivity to the main drivers and the robustness with respect to other parameters (number of frames, signal-to-noise ratio, shift amplitudes or aliasing). A number of 30 scenes with various content (urban, sea, forest, mountains …) has been selected from the image databank. The performance analyses are based on a set of quantitative criteria: LPIPS [20], PSNR [21] as well as human visual evaluation. The robustness curves obtained for the number of frames are given below.

3.4.1.1 Impact of the number of frames

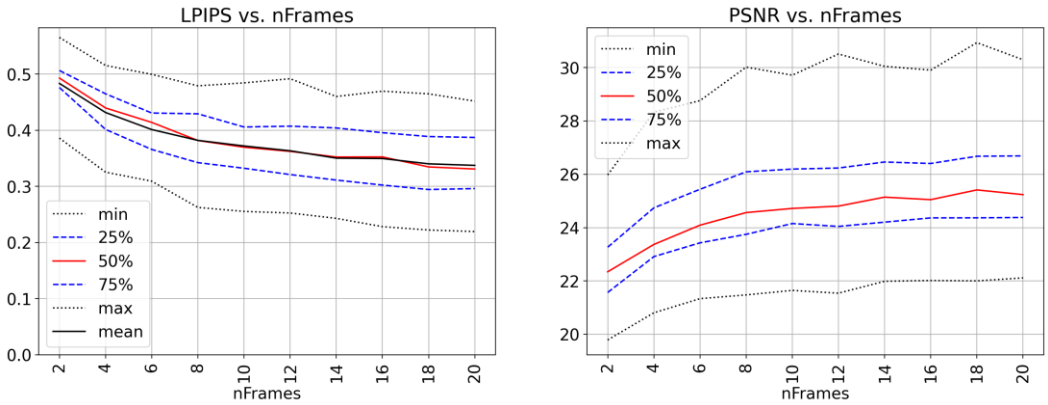

Figure 18: Robustness of the Google + deconvolution + denoising algorithm with respect to the number of frames available to perform the super-resolution process. Higher values of PSNR (resp. lower values of LPIPS) indicate better performance.

The following images show one of the results of the algorithm, for a sea city scene using different number of images to create the SR image.

Figure 19: Effect of increasing the number of frames from 10 (left) to 20 (middle), as compared to the HR reference image (right). The denoising effect on flat regions helps to reveal ships in the sea in the lower right corner.

3.4.1.2 Moving objects

As another example, we consider the case of a moving object within the frames sequence. To do so, we select a scene from the database for which acquisitions at two different time instants are available. The cloud coverage differs between acquisitions, allowing us to generate a 'corrupted' frame with clouds that are not present in the rest of the sequence. The goal of this simulation is to test the robustness module of the algorithm.

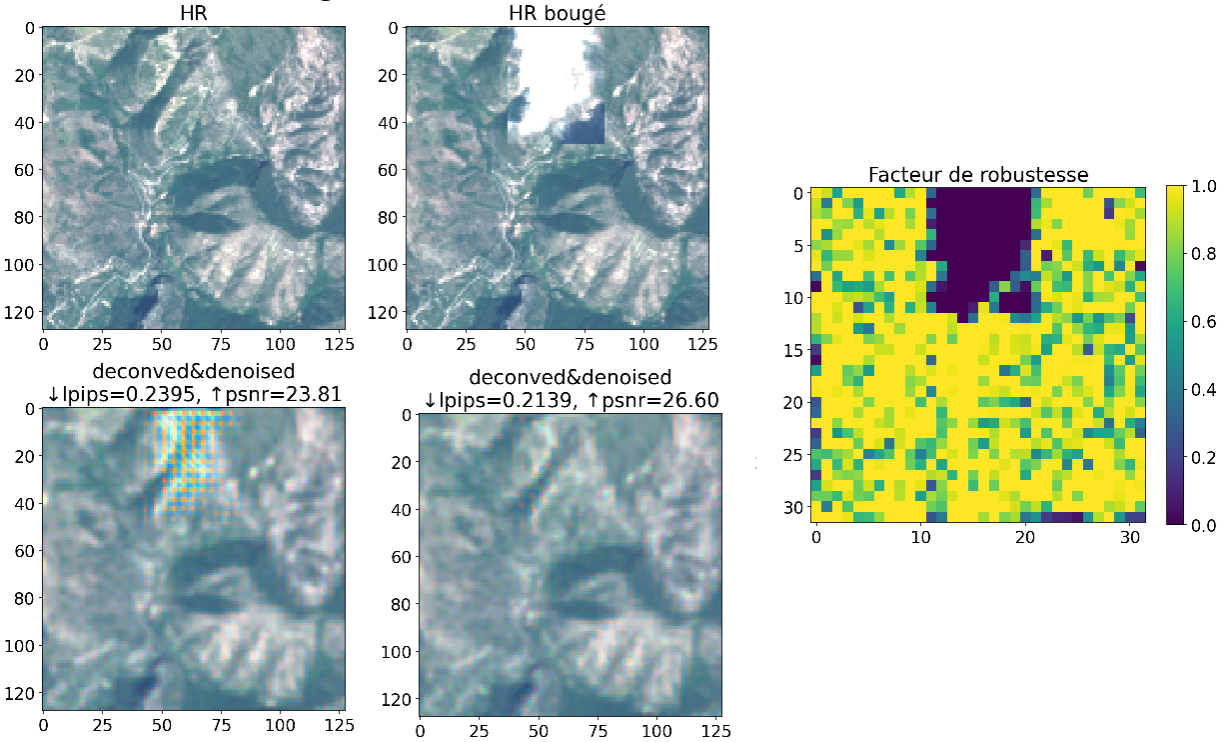

Figure 20 : Left: HR image, cloud location, reconstruction without and with the reconstruction module activated. Right: estimated robustness mask: the contribution of pixels corresponding to the cloud is set to zero by the algorithm.

When the results are given without the robustness module, strong artefacts are present in the cloud region, indicating that the kernel regression fails to estimate the correct fusion weights. However, when the robustness module is activated, the cloud is correctly detected and the contribution of pixels in this region is set to zero.

4 CONCLUSIONS & RECOMMENDATIONS

The work presented provides a full application of the line-of-sight stabilization for two missions of LEO and GEO Earth Observation, involving conventional inertial based stabilization and digital stabilization with a super resolution approach. The digital stabilization simulation campaign confirmed the expected performance over a variety of parameters (illumination conditions, SNR, scene types, etc.), and the sensitivity to the main design drivers has been assessed. The performance of SR is better than naïve interpolation which is already compliant to the SNR requirement. In addition, the blurring from pointing stability and overall Image Quality is deemed fine although the usual MTF requirement does not apply. For the push-broom interferometer scenario, the campaign confirmed the expected performance, and it is compliant to the requirements for scan step and stare, and slow down maneuvers and it enabled to characterize the sensitivity to the main design drivers and disturbances, such as FSM noise, gyroscope noise and S/C pointing stability. The opto-mechanical stabilization enabled us to reach a pointing stability and the agility required. For digital stabilization, the equivalent stability is in the order of 1-5% of a pixel, corresponding to 10-50nrad over 100ms. In conclusion, the study has paved the way for the future use of line-of-sight stabilization systems by increasing the understanding and the maturity of such systems, for agile line of sight control and digital stabilization.

5 ACKNOWLEDGEMENT

The results presented in this paper have been achieved under funding by the ESA Line of sight stabilization techniques and High accuracy Image stabilization Breadboarding studies 4000133400/20/NL/CRS and 4000126060/18/NL/FE. The view expressed in this paper can in no way be taken to reflect the official opinion of the European Space Agency.

6 REFERENCES

[1] Line of Sight Stabilization Techniques, ESA contract 4000133400/20/NL/CRS, Final Report, Thales Alenia Space, Ref: ISABELA_FR
[2] High Accuracy Image Stabilization Breadboarding, ESA contract 4000126060/18/NL/FE, Final Report, Thales Alenia Space, Ref: ISABELA_FR
[3] High accuracy image stabilization system for GEO High Resolution mission - Preliminary design and performance assessment, ESA contract 4000119980/17/NL/LF, Final Report 0005-0011724772, 14/02/2020
[4] A mission concept for real time monitoring by high resolution imaging from geostationary orbit GEO – HR, ESA contract 4000110692/14/NL/CT, TAS-F Final Report TASF-15-0006611539 Issue 2, 01/07/2016
[5] Fast loop image processing for line-of-sight accurate pointing, ESA contract 4000118131/10/NL/GLC/fk, Final Report, Thales Alenia Space, Ref: 0005-0013762844.
[6] *Essentials of Robust Control*, K. Zhou, and J. Doyle. Prentice-Hall, (1998)
[7] A. Bruhn, J. Weickert, Lucas/Kanade Meets Horn/Schunck: Combining Local and Global Optic Flow Methods, IJCV, 2005
[8] L. Meza, et al., Line of sight stabilization for the James Webb Space Telescope, AAS 05-002.
[9] T. Shimizu, Image Stabilization System for Hinode (Solar-B) Solar Optical Telescope, Solar Phys (2008)
[10] M. Meftah et al., The PICARD/SODISM Pointing Mechanism: From the Design to the Flight Performances, 14th European Space Mechanisms & Tribology Symposium – ESMATS 2011' Constance, Germany, 28–30 September 2011.

[11] R. Sánchez Maestro et al, AOCS solution to Euclid's highly stringent pointing and stability performance requirements, ESA GNC 2017: 10th International ESA Conference on Guidance,
[12] Navigation & Control Systems, May 2017 O. Rouat, Meteosat Third Generation Fine Pointing Mode Design, ESA GNC 2014: 9th International ESA Conference on Guidance, Navigation & Control Systems, June 2014
[13] D. Carter et al, GOES-16 On-Orbit Dual Isolation Performance Characterization Results, ESA GNC 2017: 10th International ESA Conference on Guidance, Navigation & Control Systems, May 2017
[14] David A. Igli, GOES-R Advanced Baseline Imager Precise Pointing Control and Image Collection, in ADVANCES IN THE ASTRONAUTICAL SCIENCES Vol. 149, AAS 13-113
[15] Sami K. Solanki et al, The Polarimetric and Helioseismic Imager for Solar Orbiter: SO/PHI, Proceedings IAU Symposium No. 305, 2015
[16] T. Staley, Lucky imaging: beyond binary stars, PhD thesis with University of Cambridge, January 2013 https://arxiv.org/abs/1404.590
[17] ESA pointing error engineering handbook, reference: ESSB-HB-E-003, 19 July 2011
[18] Wronski, Bartlomiej, et al. "Handheld multi-frame super-resolution." *ACM Transactions on Graphics (ToG)* 38.4 (2019): 1-18.
[19] Sun, Deqing, Stefan Roth, and Michael J. Black. "A quantitative analysis of current practices in optical flow estimation and the principles behind them." *International Journal of Computer Vision* 106 (2014): 115-137.
[20] Jo, Younghyun, Sejong Yang, and Seon Joo Kim. "Investigating loss functions for extreme super-resolution." *Proceedings of the IEEE/CVF conference on computer vision and pattern recognition workshops*. 2020.
[21] Huynh-Thu, Quan, and Mohammed Ghanbari. "Scope of validity of PSNR in image/video quality assessment." Electronics letters 44.13 (2008): 800-801.
[22] S. Petit Poupart et al, On ground demonstrator of digital stabilization for high resolution Earth observation Time of Delay Integration imaging, ICSO 2018: 12th International Conference on Space Optics, October 2018
[23] C. Thiebaut et al, Real-time implementation of digital stabilization for high-resolution Earth observation imaging, Proc. SPIE 10430, High-Performance Computing in Geoscience and Remote Sensing VII, 1043004, October 2017
[24] S. Baker et al, Limits on Super-Resolution and how to break them, IEEE Transactions on Pattern Analysis and Machine Intelligence, Vol. 24, No. 9, September 2002
[25] Super-Resolution image reconstruction: A technical overview, IEEE Signal Processing magazine, May 2003
[26] ALAZARD, D. Satellite Dynamics Toolbox (SDT). [online]. 2020. [Accessed 4 October 2020]. Available from: https://personnel.isae-supaero.fr/daniel-alazard/matlab-packages/satellitedynamics-toolbox.html?lang=fr
[27] ALAZARD, D.; SANFEDINO, F. Satellite dynamics toolbox for preliminary design phase. In: 43rd Annual AAS Guidance, Navigation and Control Conference, 30 January 2020 – 5 February 2020 (Breckenridge, Colorado, USA)